Fast fabrication of long-range ordered porous alumina membranes by hard anodization

WOO LEE*, RAN JI, ULRICH GÖSELE AND KORNELIUS NIELSCH

Max Planck Institute of Microstructure Physics, Weinberg 2, D-06120 Halle, Germany
*e-mail: woolee@mpi-halle.de

Nanoporous anodic aluminium oxide has been widely used for the development of various functional nanostructures. So far these self-organized pore structures could only be prepared within narrow processing conditions. Here we report a new oxalic-acid-based anodization process for long-range ordered alumina membranes. This process is a new generation of the so-called 'hard anodization' approach that has been widely used in industry for high-speed fabrication of mechanically robust, very thick ($>100\,\mu m$) and low-porosity alumina films since the 1960s. This hard anodization approach establishes a new self-ordering regime with interpore distances, $(D_{int}) = 200\text{–}300\,nm$, which have not been achieved by mild anodization processes so far. It offers substantial advantages over conventional anodization processes in terms of processing time, allowing 2,500–3,500% faster oxide growth with improved ordering of the nanopores. Perfectly ordered alumina membranes with high aspect ratios ($>1,000$) of uniform nanopores with periodically modulated diameters have been realized.

Anodic aluminium oxide (AAO) films formed by the electrochemical oxidation of aluminium have been investigated and used in numerous products for more than 100 years[1–7]. In recent years, nanoporous AAO with a hexagonal arrangement of monodisperse nanopores has become a popular template system for the synthesis of various functional nanostructures[8–14]. This trend originated from the discovery of self-ordered alumina membranes by Masuda and Fukuda[15] in 1995. In general, the fabrication of self-ordered Al_2O_3 pore arrays, under conventional so-called 'mild anodization' (MA) conditions, requires several days of processing time and the self-ordering phenomenon occurs only in narrow process windows, known as 'self-ordering regimes'[15–21]. Owing to the slow oxide growth rates (for example, $2\text{–}6\,\mu m\,h^{-1}$), MA processes based on Masuda's approach have not been used in industrial processes so far. For practical applications, simple and fast fabrication of highly ordered AAO with a wide range of pore sizes and interpore distances would be highly desirable.

In this paper we draw renewed attention to the so-called 'hard anodization' (HA) process, which was invented in the early 1960s[22–25]. The HA process is characterized by the use of sulphuric acid at relatively low temperatures and high current densities, and has been widely used for various industrial applications (for example, surface finishing of aluminium cookware, automobile engineering, textile machinery and so on) by taking advantage of the high-speed oxide growth ($50\text{–}100\,\mu m\,h^{-1}$) (refs 26–29). In academic research, however, the HA process has not been favoured over the past four decades and has not been applied to the development of nanostructured materials because of difficulties in controlling important structural parameters, such as pore size, interpore distance and the aspect ratio of the nanopores of the resulting alumina membranes.

In typical MA processes, self-ordered arrays of alumina nanopores can be obtained within three well-known growth regimes: (1) sulphuric acid (H_2SO_4) at 25 V for an interpore distance $(D_{int}) = 63\,nm$ (refs 16,17), (2) oxalic acid ($H_2C_2O_4$) at 40 V for $D_{int} = 100\,nm$ (refs 15,17,20), and (3) phosphoric acid (H_3PO_4) at 195 V for $D_{int} = 500\,nm$ (refs 18,21). When

741

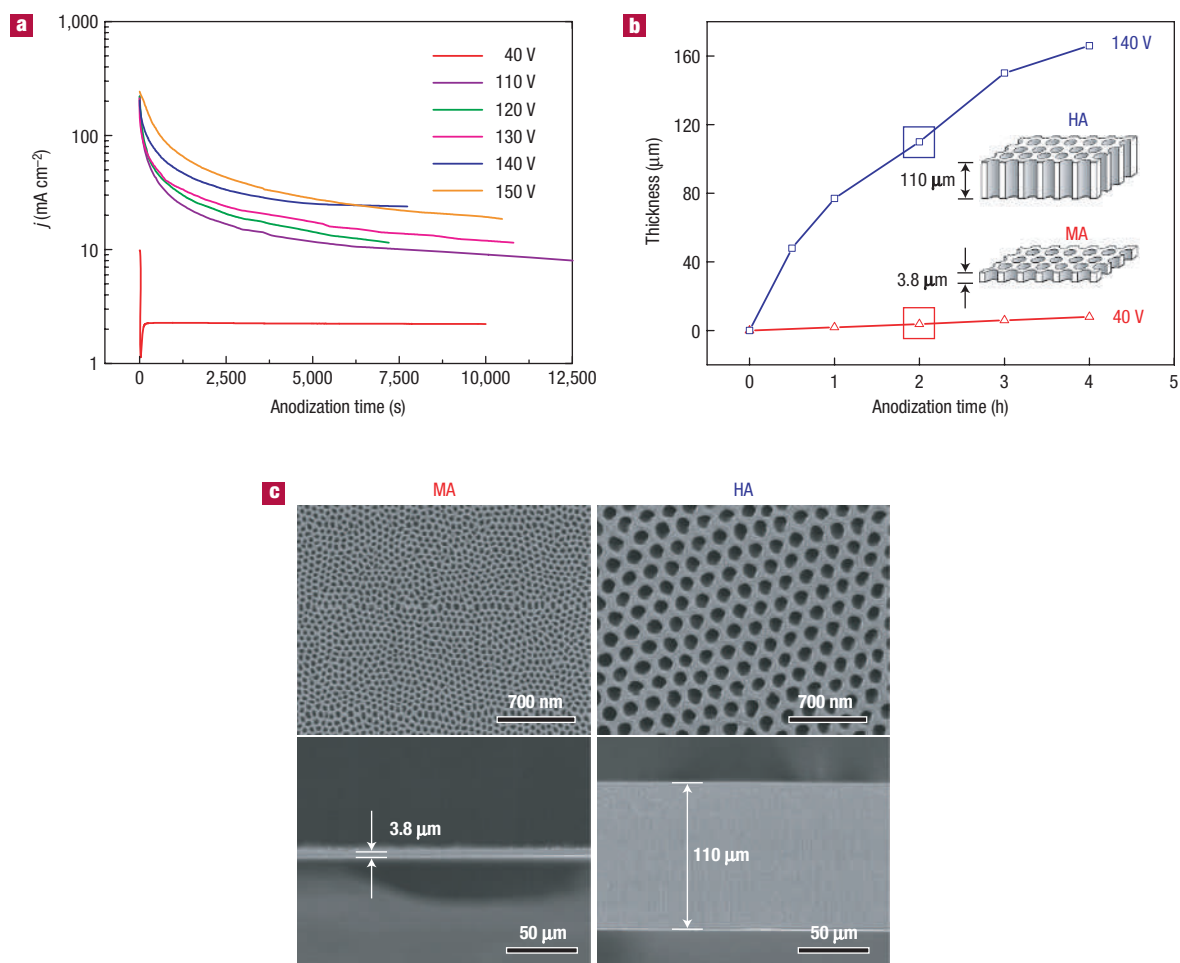**Figure 1 Hard anodization versus mild anodization. a**, Current–time transients during HA of electropolished aluminium substrates in 0.3 M $H_2C_2O_4$ (1 °C). The current–time transient of a conventional MA (0.3 M $H_2C_2O_4$, 1 °C, 40 V) is also plotted (red line) for comparison. **b**, Film thickness as a function of time during HA at 140 V (blue line) and an MA process at 40 V (red line). The different thicknesses of anodic oxides after 2 h of anodization are highlighted schematically in the insets. **c**, SEM micrographs of the corresponding AAO specimens formed by MA for 2 h (left column) and HA for 2 h (right column). The arrangements of pores for the respective samples are shown in the upper SEM micrographs. The thicknesses of the respective samples are indicated in the cross-sectional SEM micrographs.

the anodization process is carried out outside the self-ordering regimes, the degree of spatial ordering decreases drastically. Applied voltages higher than the optimum value required to maintain stable anodization in a given electrolyte always result in 'breakdown' or 'burning' of the oxide film caused by catastrophic flow of electric current[30]. These process limitations reduce the potential applications of nanoporous alumina. Substantial efforts have been made to explore new self-ordering regimes in a wider range of D_{int} (refs 19,30–33). Shingubara et al.[19] used a 1:1 oxalic/sulphuric acid mixture in anodic oxidation to obtain self-ordered nanopore arrays with $D_{int} = 73$ nm. Ono et al. found that domains of highly-ordered pore arrays occur in porous alumina film formed during breakdown[30,32]. More recently, Chu et al.[31] reported the fabrication of self-ordered AAO in sulphuric acid solution under high anodization potentials and current densities of up to 70 V and 200 mA cm^{-2}, far from the MA regime (H_2SO_4: 25 V and 2–4 mA cm^{-2}) but similar to the anodization conditions for HA[22,23,25,34,35]. They named this process 'high-field anodization' and used an 'aged sulphuric solution'. A combination of lithography pre-patterning of the aluminium surfaces and subsequent MA

has also provided some degree of flexibility in controlling D_{int} (refs 13,36–39) and the pore arrangement. However, this MA-based approach also has limitations in fabricating AAO membranes with a high aspect ratio (depth divided by the diameter) of nanopores above about 20.

We report a new self-ordering regime of nanoporous AAO that was found during HA of aluminium substrates using oxalic acid and applying potentials of 100–150 V, which are more than three times higher than the voltage (40 V) used in conventional oxalic acid anodization[15,20]. On the basis of the newly found self-ordering behaviour, we have realized the fabrication of novel AAO membranes with periodically modulated diameters of nanopores, whose three-dimensional (3D) pore structures have the potential for a broad range of nanotechnology applications, such as 3D photonic crystals, meta-materials, microfluidics and for the template-based synthesis of multifunctional nanowires and nanotubes with modulated diameters.

To suppress breakdown effects and to enable uniform oxide film growth at a high voltage (>100 V), we found that an oxide layer (thickness >400 nm) should be formed on the surface of
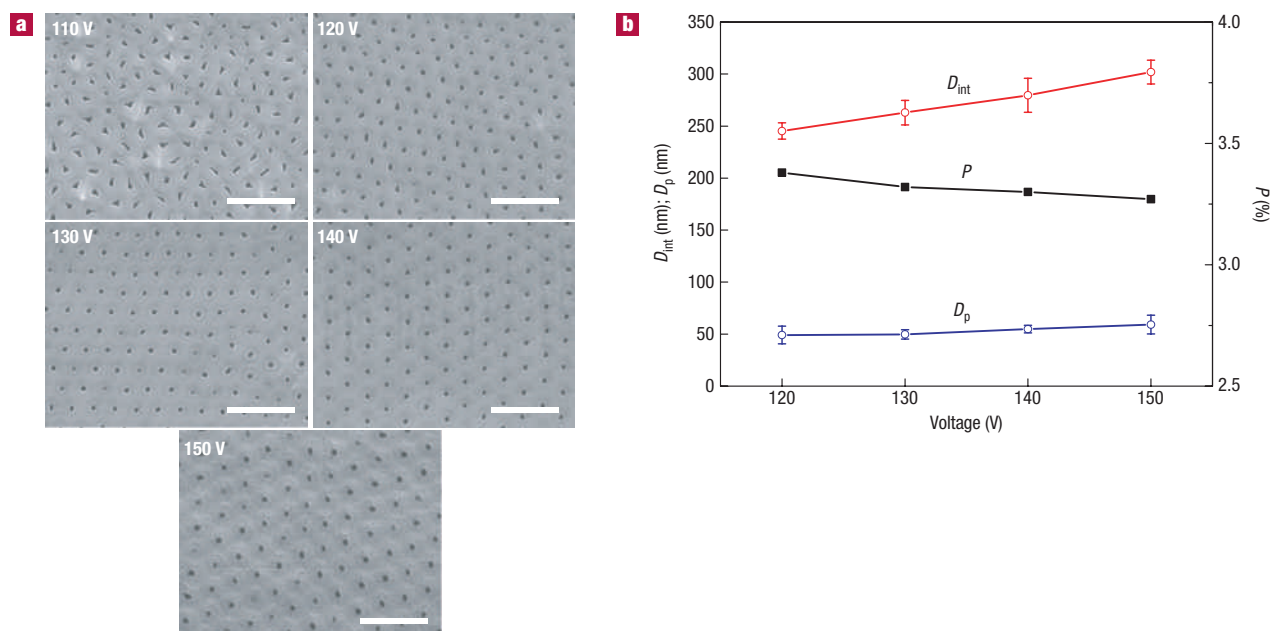
Figure 2 The effect of voltage on the self-ordering of AAO. a, Surface SEM micrographs of self-ordered AAOs formed in HA at voltages specified in the respective micrographs (scale bars = 800 nm). HA of a mirror-finished aluminium substrate carried out using 0.3 M $H_2C_2O_4$ (1 °C) for 160 min. This SEM investigation was carried out on the bottom surfaces of the resulting AAOs after the removal of the barrier layer by ion milling. **b**, The evolution of interpore distance (D_{int}), pore diameter (D_p) and porosity (P) as a function of the HA voltage. The porosity (P) of AAO was estimated using the following equation assuming an ideal hexagonal arrangement of the pores; $P = (\pi/2\sqrt{3})(D_p/D_{int})^2$, where D_p and D_{int} denote the pore diameter and the interpore distance (or cell size), respectively. The error bars represent the standard deviations from the mean of each measured quantity.

the aluminium substrate before carrying out the HA process. This protective oxide layer can be generated by anodizing an aluminium substrate under MA conditions using, for example, 0.3 M oxalic acid at 40 V for 5–10 min. Subsequently, the anodization voltage is slowly increased to a target formation voltage (100–150 V) for HA at a rate of 0.5–0.9 V s^{-1} and the HA will be continued under a constant potential. It is believed that the surface oxide layer provides uniform pore nucleation sites at the early stage of high-voltage anodization, preventing local catastrophic events such as local flow of high electrical current and defects by surface pitting (see Supplementary Information, Fig. S1). The HA is accompanied by a large evolution of heat, which is effectively removed using an appropriate electrochemical setup in our experiment (see Supplementary Information, Fig. S2).

The evolution of the current and the thickness of the AAO film were investigated for HA at 110–140 V and MA at 40 V using 0.3 M $H_2C_2O_4$ (Fig. 1). Unlike the typical anodization curves for MA (red line in Fig. 1a), the current–time transients in HA show a nearly exponential decrease as a function of time. Such an unusual behaviour of the current transition for HA can be explained by the diffusion-limited electrochemical oxidation of aluminium at the pore bottom as a result of the extremely rapid and homogeneous film growth (50–70 μm h^{-1}) on the whole sample area. It is believed that the anodization current is mainly related to the movement of ionic species (O^{2-}, OH$^-$, Al^{3+}) through the oxide layer at the bottom of the pores[40–42]. The mass transport of oxygen-containing anionic species from the bulk reservoir (that is, the electrolyte) to the oxide/metal interface determines the current density during the anodization process. Accordingly, the ionic current is expected to gradually decrease over time due to the extended diffusion path along the nanopores. The diffusion-limitation of the HA process is further confirmed by the nonlinear film growth rate (see Fig. 1b

and Supplementary Information, Fig. S3). The HA process offers a big advantage over conventional anodization processes in terms of considerably shortened fabrication times due to the high-speed film growth rate (Fig. 1c).

Investigations of the pore arrangement revealed that the cell homogeneity of the AAO films increases dramatically as soon as the anodization voltage is higher than 110 V (Fig. 2a). The most highly ordered AAO films were obtained under 120–150 V, where the cell ordering is insensitive to the anodization potential. According to scanning electron microscopy (SEM) analyses, the typical size of the ordered domains is in the range of 6–8 μm. The degree of self-ordering of oxide nanopores decreased as the anodization potential approached 155 V, which is the maximum anodization voltage that could be applied avoiding breakdown.

The effects of anodization voltages on the self-ordering of the AAO films are shown in Fig. 2b. The interpore distance (D_{int}) and pore size (D_p) are found to be linearly proportional to the anodization voltage, similar to the MA process[1,40]. The porosity (P) of self-ordered anodic alumina films formed by HA is $P_{HA} = 3.3–3.4\%$. This value is about one-third of the porosity value ($P_{MA} \sim 10\%$) that we previously proposed as a requirement for self-ordered AAO under MA conditions[21]. On the basis of the observations on porous oxide films formed by breakdown anodization, Ono et al.[30] recently suggested that the porosity value of $P \sim 10\%$ is the optimum and also the minimum value. However, our results show that this argument is not applicable to AAO films formed by the HA process.

Figure 3 shows the relationship between D_{int} and the anodization voltage for HA. The self-ordering voltages and the corresponding D_{int} that have been reported for MA processes are also plotted for comparison. It should be pointed out that the present HA process establishes a new self-ordering regime in the
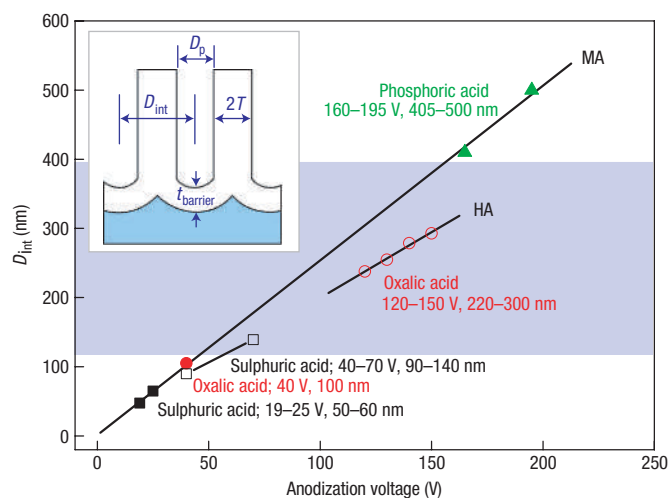
Figure 3 A new and second regime of self-ordering for oxalic acid anodization. Summary of self-ordering voltages and corresponding interpore distance (D_{int}) in conventional MA in sulphuric (filled black squares)[16,17], oxalic (filled red circle)[15,17,20] and phosphoric acid (filled green triangle)[18,21], together with recently reported results by Chu *et al.* (open black squares)[31]. The black solid line represents the linear regression of the data with a correlation parameter of $\zeta_{MA} = 2.5\ nm\,V^{-1}$. The coloured background for $100\ nm < D_{int} < 400\ nm$ represents the self-ordering regime unexplored until now. The interpore distance (D_{int}) versus anodization voltage observed in oxalic HA is plotted (red open circles) with the corresponding regression line (black solid line). The correlation parameter estimated from the linear regression is $\zeta_{HA} = 2.0\ nm\,V^{-1}$. The inset shows the schematic cross-section of the porous alumina structure with the barrier layer; D_{int} = interpore distance, D_p = pore diameter, T = thickness of the pore wall, $t_{barrier}$ = thickness of the barrier layer.

Table 1 MA versus HA in 0.3 M $H_2C_2O_4$ (1 °C).

	MA	HA
Voltage (V)	40	110–150
Current density (mA cm^{-2})	5	30–250
Film growth rate (μm h^{-1})	2.0 (linear)	50–70 (nonlinear)
Porosity (P; %)	10	3.3–3.4
Interpore distance (D_{int}; nm)	100	220–300
Pore diameter (D_p; nm)	40	49–59
Pore density (ρ; pores cm^{-2})*	1.0×10^{10}	1.3–1.9×10^9
ζ (nm V^{-1})†	2.5	2.0
Water contents (wt%)	0.3–0.4	0.1
Carbon contents (wt%)	2.4	1.8
Density (g cm^{-3})	2.8	3.1

* Pore density (ρ) = $(2/\sqrt{3}D_{int}^2) \times 10^{14}$ cm^{-2}.

† Proportionality constant correlating the interpore distance (D_{int}) of self-ordered anodic alumina with the anodization voltage.

ranges of $D_{int} = 200$–$300\ nm$, filling the gap that has not been achieved by conventional MA processes. Previous studies indicate that D_{int} of AAO formed under ordinary MA conditions using H_2SO_4, $H_2C_2O_4$ and H_3PO_4 is linearly dependent on the applied voltage with a proportionality constant $\zeta_{MA} = 2.5\ nm\,V^{-1}$ (refs 1, 40,43). However, the proportionality constant $\zeta_{HA} = 2.0\ nm\,V^{-1}$ for AAO films formed by the HA process is lower than that for the MA processes. The reduced ζ for HA could be attributed to a reduced voltage dependence of the pore diameter (D_p) and the barrier layer thickness ($t_{barrier}$) of anodic alumina under high current density (that is, high electric field (E) at the pore bottom). The voltage dependence of D_{int} can be expressed by $D_{int} = \zeta U = [C_{pore} + C_{wall} t_{barrier}]U$, where $C_{pore} U$ and $C_{wall} t_{barrier} U$ respectively represent the potential (U) dependence of the pore diameter ($D_p = C_{pore} U$) and the wall thickness ($T = C_{wall} t_{barrier} U$) of alumina nanopores with proportionality constants C_{pore}, C_{wall} (see inset of Fig. 3).

According to microscopic analyses, the barrier layer thickness for HA increases at a rate of $t_{barrier}^{HA} \sim 1.0\ nm\,V^{-1}$, which is $\sim$20% smaller than $t_{barrier}^{MA} \sim 1.3\ nm\,V^{-1}$ for MA processes[1,2]. The reduced $t_{barrier}^{HA}$ could be attributed to the high current density (j) involved in the HA process in accordance with the high field conductivity theory[44,45]; for valve metals, the current density (j) can be related to the potential drop (ΔU) across the barrier layer of thickness $t_{barrier}$: $j = j_0 \exp(\beta \Delta U / t_{barrier})$, where j_0 and β are material-dependent constants at a given temperature and $\Delta U / t_{barrier}$ is the effective electric field strength (E) across the barrier layer. For a given anodization potential, the barrier layer thickness ($t_{barrier}$) is inversely proportional to the logarithm of current density (j). We observed differences in the chemical compositions of AAO films formed by

HA and MA (see Supplementary Information, Fig. S4). According to quantitative analyses on carbon and water contents, hard anodized samples showed a lower level of impurities, which might explain the higher density of anodic alumina formed by the HA process (Table 1). In addition, the differences in impurity levels could influence the electrical and optical properties of the anodic alumina films. In fact, the AAO films formed by HA (>100 V) were bright yellow, whereas AAO films prepared by MA (40 V) are transparent. Strong fracture behaviour has been reported for anodic alumina formed in concentrated sulphuric acid solution at high potentials (25–70 V)[31,34,35]. These pore structures exhibit weak cell junctions and the separation of individual alumina nanotubes by weak mechanical forces. For the HA pore structures formed in oxalic acid we observed very solid cell junctions. Like MA-anodized alumina membranes, the cracks propagate across the nanopores when strong mechanical forces are applied.

The microscopic analysis indicated that the pore diameter (D_p^{HA}) of anodic alumina for HA increases at a rate of $C_{pore}^{HA} = 0.4\ nm\,V^{-1}$, which is 55% lower than $C_{pore}^{MA} = 0.9\ nm\,V^{-1}$ for MA. For a given anodization potential, the HA process yields anodic alumina with a smaller D_p. It is reported that D_p is strongly affected by the dissolution velocity of alumina that is determined by the pH value at the pore bottom[42]. For HA, the reduced D_p could be explained by enhanced proton activity at the pore bottom, where significant Joule heating occurs as a result of the high current density (that is, high electric field E).

It can be assumed that the rapid oxide formation due to the high current density will generate a high mechanical stress at the metal/oxide interface due to the associated volume expansion[40,41]. Under this energetically unfavourable condition, the anodization will proceed in such a way that the resulting mechanical stress is minimized. This can be achieved by reducing the cell size to enlarge the surface area of the metal/oxide interface. The ion mobility within the barrier oxide and the degree of field-stimulated local oxide dissolution should be adjusted accordingly. Because the interfacial stress increases with the oxide growth rate at the metal/oxide interface[40,41], the size of the cells should decrease with current density for a given anodization voltage. Therefore, ζ_{HA} for anodic alumina formed by HA should be smaller than that for AAO formed by MA. It is also expected that the high interfacial stress gives rise to a repulsive force between the pore cells at the barrier layer. In analogy to MA, we propose that the repulsive interactions are the main driving force for the self-organized formation of the hexagonal pore arrays[40,41]. In other words, the high current density in HA plays an important role in determining the self-ordering of the oxide nanopores as well as the cell size.
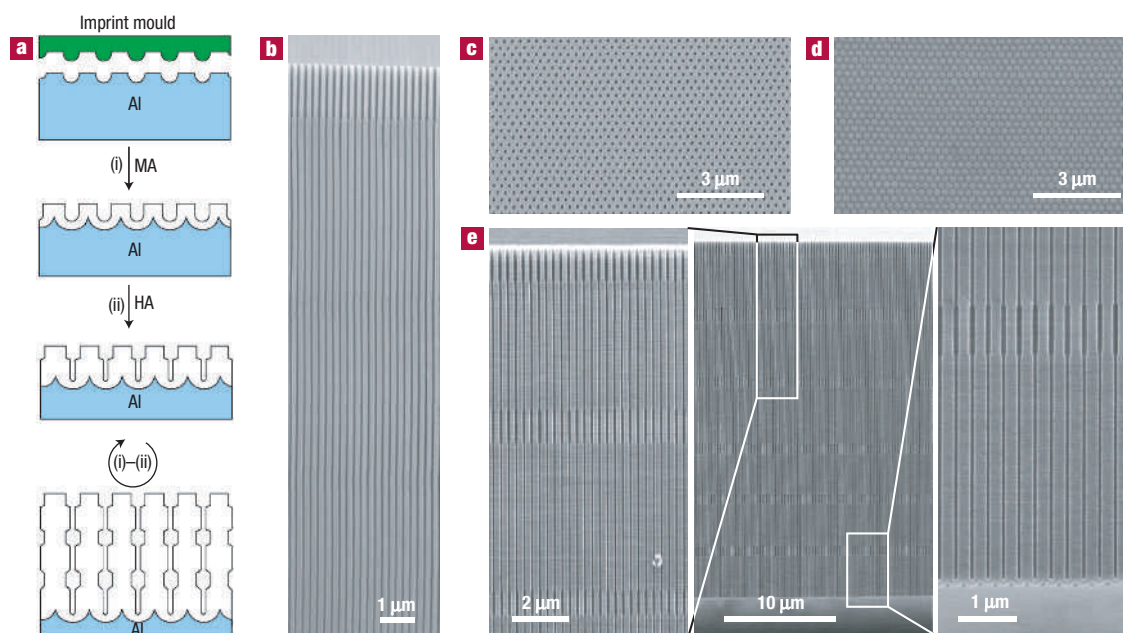
Figure 4 Long-range ordered alumina membranes with modulated pore diameters. a, Scheme for the fabrication of porous alumina with modulated pore diameters by a combination of MA and HA of a pre-patterned aluminium substrate. **b,** SEM micrograph showing a cross-section of anodic alumina ($D_{int} = 210$ nm) with an ultra-high aspect ratio ($>1,000$) of uniform nanopores; the HA on pre-patterned aluminium ($D_{int} = 210$ nm) was conducted at 110 V. **c,d,** SEM micrographs showing the top and bottom surface view of the as-prepared anodic alumina ($D_{int} = 275$ nm) with perfect hexagonal arrangement of the nanopores. **e,** SEM micrographs showing the cross-section view of the corresponding sample with modulated pore diameters. Magnified cross-section images of the top and bottom parts of the membrane are shown on the left and right, respectively.

Because the current density decreases exponentially with time (Fig. 1a), it is expected that the cell size (or D_{int}) should increase with anodization time. Investigations of D_{int} as a function of anodization time at 140 V revealed that the average D_{int} of the samples actually increases with anodization time for the first 30 min (see Supplementary Information, Fig. S5). The initial increase in D_{int} could be ascribed to the rapid drop in current density at the early stage of HA, and supports the idea that the current density (that is, electric field strength E across the barrier layer at the pore bottom) is a key parameter governing D_{int} in HA. On the other hand, the variation in the average D_{int} was found to be insensitive to the anodization time for samples anodized for more than 40 min, where the current density is rather stable (see Supplementary Information, Fig. S5). All of these experimental findings suggest that the current density needs to be maintained at a certain level to obtain long-range ordered anodic alumina with a desired D_{int} at a given anodization voltage.

The arguments raised above were further evidenced by realizing the fabrication of monodomain AAO membranes with a high aspect ratio of uniform nanopores by HA. For MA processes, it is well established that pre-patterning the aluminium substrates before the anodization initiates the pore nucleation and guides the growth of nanopores during anodization[13,36–38]. AAO membranes with ideally ordered pore arrangements in a wide range of intervals have been prepared using this approach[37]. However, the attainable maximum aspect ratio of the nanopores maintaining the initial periodic arrangement critically depends on the anodization conditions[36,38]. Anodic alumina with a high aspect ratio of uniform nanopores can only be prepared within limited processing windows, satisfying self-ordering conditions[15–18,20,21]. For MA of pre-patterned aluminium using oxalic acid, high aspect ratios ($>1,000$) of nanopores could be obtained at 40 V. Under other anodization voltages, the ideal ordering of the nanopores can only be maintained up to several micrometres in depth (aspect ratio <20), and became perturbed as the thickness of the oxide increased.

We found that the HA process can overcome such limitations. AAO membranes with uniform nanopores with aspect ratios of more than 1,000 were prepared by HA in the broad self-ordered regime of oxalic acid (see Fig. 4b and Supplementary Information, Fig. S6). In addition, on the basis of the fact that HA yields anodic alumina with one-third lower porosity than MA (that is, $P_{HA} \sim 3\%$ for HA and $P_{MA} \sim 10\%$ for MA), we were able to modulate nanopore diameter by combining both anodization processes (Fig. 4). Initially, the surface of the electropolished aluminium was pre-patterned using an imprint stamp with hexagonal arrays of imprint tips with 275 nm period[39] (Fig. 4a). Subsequently, the resulting aluminium was anodized under MA conditions at 110 V using 4 wt% H_3PO_4 (10 °C) for 15 min, resulting in a segment of oxide nanopores with higher porosity. Subsequently, HA was carried out at 137 V using 0.015 M $H_2C_2O_4$ (0.5 °C) for 2 min, resulting in a lower porosity nanoporous alumina segment. During HA, the current density was maintained at the range of 33–35 mA cm^{-2} by adding fresh 0.3 M $H_2C_2O_4$ into the anodization cell. The anodization voltage was chosen based on the linear relation between D_{int} and the anodization voltage; $\zeta_{MA} = 2.5$ nm V^{-1} for MA[1,40,43] and $\zeta_{HA} = 2.0$ nm V^{-1} for HA. These two anodization processes constitute one modulation period in the oxide nanopores. Highly uniform periodic modulations in pore diameters have been achieved by repeating two consecutive anodization processes of MA and HA (Fig. 4e). The length of each segment of oxide nanopores can freely be controlled by varying the anodization time of the anodization process. The maintenance of the ideal hexagonal arrangement (Fig. 4c) of nanopores was

verified by SEM investigation of the bottom surface of the oxide membrane, showing the ideally ordered configuration of barrier layers (Fig. 4d). Anodic alumina with a high aspect ratio ($>1,000$) of uniform parallel nanopores ($D_{int} = 210$ nm) could also be fabricated by a continuous HA process (Fig. 4b).

Finally, from a practical point of view, the HA process has many advantages over conventional MA as summarized in Table 1. We believe that these findings on the self-ordering phenomenon during HA will lead to a revitalization of the HA processes in nanotechnology research as well as in industry. Our major findings on the HA with oxalic acid are as follows. (1) The current density (that is, the electric field strength E at the pore bottom) is an important parameter governing the self-organization of oxide nanopores in a given anodization potential. (2) A new self-ordering regime is established over a broad range of interpore distance $D_{int} = 200–300$ nm. (3) The ratio ζ between the interpore distances D_{int} and the anodization potential is lower ($\zeta_{HA} = 2.0$ nm V^{-1} for HA, $\zeta_{MA} = 2.5$ nm V^{-1} for MA). (4) The porosity P is lower ($P_{HA} \sim 3\%$, $P_{MA} \sim 10\%$). (5) The growth rate of the porous oxide film is 25–35 times larger (>50 µm h^{-1}) than for MA. (6) Ideally ordered alumina membranes with a high aspect ratio ($>1,000$) of uniform nanopores can be fabricated by HA of pre-patterned aluminium. (7) A combination of HA and MA allows modulation of the pore diameter over extremely high aspect ratios.

METHODS

SURFACE PRE-TREATMENT OF THE ALUMINIUM FOILS

As-received aluminium plates (Goodfellow, 99.999%) were used in the anodization experiments without the annealing step. The aluminium substrates were electrochemically polished in a 1:4 solution of 65% HClO$_4$ and 99.5% ethanol (5 °C) to exclude effects (for example, localized field concentration) that could arise from the surface roughness during HA. During the electropolishing process, the electrolyte was vigorously stirred.

HA OF ALUMINIUM

All HA experiments were carried out using an electrochemical cell equipped with a cooling stage (see Supplementary Information, Fig. S2). To achieve uniform film growth in oxalic acid solution (H$_2$C$_2$O$_4$, Aldrich) under high voltages (>100 V), a mirror-finished aluminium plate was first anodized at 40 V in 0.3 M H$_2$C$_2$O$_4$ (1–2 °C) for 8 min. This pre-anodization step produced a thin porous oxide layer (about 400-nm thick) on the surface of the aluminium substrate. Then, the anodization voltage was gradually increased to a target formation voltage (100–160 V) at the rate of 0.5–0.9 V s^{-1}. A steady increase in current density was observed during the increase in the anodization voltage. When the electric field reached the target formation voltage, the current density decreased exponentially as a function of time. Direct anodization without this pre-anodization resulted in non-uniform oxide films biased by extremely high and inhomogeneous current flow (>250 mA cm^{-2}) (see Supplementary Information, Fig. S1).

HA is accompanied by a large evolution of heat due to the high anodic current associated with the high electric field at the barrier oxide. The excessive heat promotes acidic dissolution of the oxide membrane by the electrolyte (H$_2$C$_2$O$_4$). Prolonged HA under such conditions results in complete collapse of the pore structure of the alumina membranes. Accordingly, the control of the heat is important. In our experiments, the heat was effectively removed using a powerful cooling stage that was in thermal contact with the aluminium substrate through a copper plate (see Supplementary Information, Fig. S2).

SURFACE PRE-PATTERNING OF ALUMINIUM

Surface pre-patterning of aluminium has been achieved using a Ni imprint stamp[39]. For the development of wafer-scale Ni imprint stamps, first we fabricated master patterns by laser interference lithography, where the period and two-dimensional arrangement of the patterns could be adjusted throughout a wide range of geometries and periodicities[39]. Ni imprint stamps could be replicated from the master patterns using an electrodeposition technique. Typically, nanoindentation of the Al was achieved by applying about 25 kN cm^{-2} for 10 s using an oil press.

References

1. Keller, F., Hunter, M. S. & Robinson, D. L. Structural features of oxide coatings on aluminium. *J. Electrochem. Soc.* **100**, 411–419 (1953).
2. Hunter, M. S. & Fowle, P. Determination of barrier layer thickness of anodic oxide coating. *J. Electrochem. Soc.* **101**, 481–485 (1954).
3. Thompson, G. E. & Wood, G. C. Porous anodic film formation on aluminium. *Nature* **290**, 230–232 (1981).
4. Lohrengel, M. M. Thin anodic oxide layers on aluminium and other valve metals: high field regime. *Mater. Sci. Eng. R* **11**, 243–294 (1993).
5. Diggle, J. W., Downie, T. C. & Goulding, C. W. Anodic oxide films on aluminium. *Chem. Rev.* **69**, 365–405 (1969).
6. Thompson, G. E., Furneaux, R. C., Wood, G. C., Richardson, J. A. & Goode, J. S. Nucleation and growth of porous anodic films on aluminium. *Nature* **272**, 433–435 (1978).
7. Wood, G. C. & O'Sullivan, J. P. The anodizing of aluminium in sulphate solutions. *Electrochim. Acta* **15**, 1865–1876 (1970).
8. Lee, W., Scholz, R., Nielsch, K. & Gösele, U. A template-based electrochemical method for the synthesis of multisegmented metallic nanotubes. *Angew. Chem. Int. Edn* **44**, 6050–6054 (2005).
9. Lee, S. B. *et al.* Antibody-based bio-nanotube membranes for enantiomeric drug separations. *Science* **296**, 2198–2200 (2002).
10. Park, S., Lim, J.-H., Chung, S.-W. & Mirkin, C. A. Self-assembly of mesoscopic metal-polymer amphiphiles. *Science* **303**, 348–351 (2004).
11. Kovtyukhova, N. I. & Mallouk, T. E. Nanowire p-n heterojunction diodes made by templated assembly of multilayer carbon-nanotube/polymer/semiconductor-particle shells around metal nanowires. *Adv. Mater.* **17**, 187–192 (2005).
12. Zhi, L., Wu, J., Li, J., Kolb, U. & Müllen, K. Carbonization of disclike molecules in porous alumina membranes: Toward carbon nanotubes with controlled graphene-layer orientation. *Angew. Chem. Int. Edn* **44**, 2120–2123 (2005).
13. Mikulskas, I., Juodkazis, S., Tomašiūmas, R. & Dumas, J. G. Aluminium oxide photonic crystals grown by a new hybrid method. *Adv. Mater.* **13**, 1574–1577 (2001).
14. Hurst, S. J., Payne, E. K., Qin, L. & Mirkin, C. A. Multisegmented one-dimensional nanorods prepared by hard-template synthetic methods. *Angew. Chem. Int. Edn* **45**, 2672–2692 (2006).
15. Masuda, H. & Fukuda, K. Ordered metal nanohole arrays made by a two-step replication of honeycomb structures of anodic alumina. *Science* **268**, 1466–1468 (1995).
16. Masuda, H., Hasegwa, F. & Ono, S. Self-ordering of cell arrangement of anodic porous alumina formed in sulphuric acid solution. *J. Electrochem. Soc.* **144**, L127–L130 (1997).
17. Li, A. P., Müller, F., Birner, A., Nielsch, K. & Gösele, U. Hexagonal pore arrays with a 50–420 nm interpore distance formed by self-organization in anodic alumina. *J. Appl. Phys.* **84**, 6023–6026 (1998).
18. Masuda, H., Yada, K. & Osaka, A. Self-ordering of cell configuration of anodic porous alumina with large-size pores in phosphoric acid solution. *Jpn. J. Appl. Phys.* **37**, L1340–L1342 (1998).
19. Shingubara, S., Morimoto, K., Sakaue, H. & Takahagi, T. Self-organization of a porous alumina nanohole array using a sulfuric/oxalic acid mixture as electrolyte. *Electrochem. Solid-State Lett.* **7**, E15–E17 (2004).
20. Li, F., Zhang, L. & Metzger, R. M. On the growth of highly ordered pores in anodized aluminium oxide. *Chem. Mater.* **10**, 2470–2480 (1998).
21. Nielsch, K., Choi, J., Schwirn, K., Wehrspohn, R. B. & Gösele, U. Self-ordering regimes of porous alumina: The 10% porosity rule. *Nano Lett.* **2**, 677 (2002).
22. Csokán, P. Beiträge zur kenntnis der anodischen oxydation von aluminium verdunnter, kalter schwefelsaure. *Metalloberfläche* **15**, B49–B53 (1961).
23. Csokán, P. & Sc, C. C. Hard anodizing: Studies of the relation between anodizing conditions and the growth and properties of hard anodic oxide coatings. *Electroplat. Metal Finish.* **15**, 75–82 (1962).
24. Lichtenberger-Bajza, E., Domony, A. & Csokán, P. Untersuchung der struktur und anderer eigenschaften von durch anodische oxydation auf aluminium erzeugten hartoxydschichten. *Werkstoffe. Korros.* **11**, 701–707 (1960).
25. Csokán, P. Some observations on the growth mechanism of hard anodic oxide coatings on aluminium. *Trans. Inst. Metal Finishing* **41**, 51–56 (1964).
26. Olbertz, B. Hartanodisieren eröffnet aluminum vielfältige technische Anwendungs-möglichkeiten. *Aluminium* **3**, 268–270 (1988).
27. Rajendra, A. *et al.* Hard anodization of aluminium and its application to sensorics. *Surf. Eng.* **21**, 193–197 (2005).
28. John, S., Balasubramanian, V. & Shenoi, B. A. Hard anodizing aluminium and its alloys—AC in sulphuric acid—sodium sulphate bath. *Met. Finish.* **82**, 33–39 (1984).
29. Hecker, J. G. Aluminum hard coats. *Product Finishing* **53**, 88–92 (1988).
30. Ono, S., Saito, M., Ishiguro, M. & Asoh, H. Controlling factor of self-ordering of anodic porous alumina. *J. Electrochem. Soc.* **151**, B473–B478 (2004).
31. Chu, S. Z., Wada, K., Inoue, S., Isogai, M. & Yasumori, A. Fabrication of ideally ordered nanoporous alumina films and integrated alumina nanotubule arrays by high-field anodization. *Adv. Mater.* **17**, 2115–2119 (2005).
32. Ono, S., Saito, M. & Asoh, H. Self-ordering of anodic porous alumina induced by local current concentration: Burning. *Electrochem. Solid-State Lett.* **7**, B21–B24 (2004).
33. Ono, S., Saito, M. & Asoh, H. Self-ordering of anodic porous alumina formed in organic acid electrolytes. *Electrochim. Acta* **51**, 827–833 (2005).
34. Arrowsmith, D. J., Clifford, A. W. & Moth, D. A. Fracture of anodic oxide formed on aluminium in sulphuric acid. *J. Mater. Sci. Lett.* **5**, 921–922 (1986).
35. Wada, K., Shimohira, T., Yamada, M. & Baba, N. Microstructure of porous anodic oxide films on aluminium. *J. Mater. Sci. Lett.* **21**, 3810–3816 (1986).
36. Masuda, H. *et al.* Square and triangular nanohole array architectures in anodic alumina. *Adv. Mater.* **13**, 189–192 (2001).
37. Fournier-Bidoz, S., Kitaev, V., Routkevitch, D., Manners, I. & Ozin, G. A. Highly ordered nanosphere imprinted nanochannel alumina (NINA). *Adv. Mater.* **16**, 2193–2196 (2004).
38. Asoh, H., Nishio, K., Nakao, M., Tamamura, T. & Masuda, H. Conditions for fabrication of ideally ordered anodic porous alumina using pretextured Al. *J. Electrochem. Soc.* **148**, B152–B156 (2001).
39. Lee, W., Ji, R., Ross, C. A., Gösele, U. & Nielsch, K. Wafer-scale Ni imprint stamps for porous alumina membranes based on interference lithography. *Small* **2**, 978–982 (2006).
40. O'Sullivan, J. P. & Wood, G. C. The morphology and mechanism of formation of porous anodic films on aluminium. *Proc. R. Soc. London A* **317**, 511–543 (1970).
41. Jessensky, O., Müller, F. & Gösele, U. Self-organized formation of hexagonal pore arrays in anodic alumina. *Appl. Phys. Lett.* **72**, 1173–1175 (1998).
42. Parkhutik, V. P. & Shershulsky, V. I. Theoretical modelling of porous oxide growth on aluminium. *J. Phys. D* **25**, 1258–1263 (1992).

43. Ebihara, K., Takahashi, H. & Nagayama, M. Structure and density of anodic oxide films formed on aluminium in oxalic acid solutions. *J. Met. Finish. Soc. Jpn* **34**, 548–553 (1983).

44. Güntherschulze, A. & Betz, H. Die bewegung der ionengitter von isolatoren bei extremen elektrischen feldstärken. *Z. Phys.* **92**, 367–374 (1934).

45. Cabrera, N. & Mott, N. F. Theory of the oxidation of metals. *Rep. Prog. Phys.* **12**, 163–184 (1948).

Competing financial interests

The authors declare that they have no competing financial interests.

Reprints and permission information is available online at http://npg.nature.com/reprintsandpermissions/